Femtosecond photoelectron spectroscopy of $I_2^-(CO_2)_n$ clusters ($n=4$, 6, 9, 12, 14, 16)

B. Jefferys Greenblatt,[a] Martin T. Zanni, and Daniel M. Neumark
Department of Chemistry, University of California, Berkeley, California 94720
and Chemical Sciences Division, Lawrence Berkeley National Laboratory, Berkeley, California 94720

(Received 10 September 1999; accepted 11 October 1999)

The photodissociation dynamics of $I_2^-(CO_2)_n(n=4-16)$ clusters excited at 780 nm have been studied with femtosecond photoelectron spectroscopy (FPES). The range of cluster sizes spans the uncaged and fully-caged product limits for this reaction. We observe time scales for a variety of processes in these clusters, including dissociation of the I_2^- chromophore, solvation of the I^- fragment, the onset of recombination on the ground state of I_2^-, vibrational relaxation, and solvent evaporation. In addition, substantial trapping in a ''solvent-separated'' state is seen for clusters with $n \geqslant 9$; this state persists for at least 200 ps, the longest time delay probed here. Simulations of the spectra were performed in order to determine the time dependence of the electronic state populations, the I_2^- vibrational distribution, and the number of CO_2 molecules in the cluster. Results are compared to previous experimental and theoretical studies of $I_2^-(CO_2)_n$ photodissociation, and to a recent FPES study of $I_2^-(Ar)_n$ clusters. © *2000 American Institute of Physics.* [S0021-9606(00)00102-1]

I. INTRODUCTION

Photoexcitation of $I_2^-(CO_2)_n$ clusters offers a powerful means for understanding the effects of solvation on a chemical reaction. The dynamics of a very simple reaction, I_2^- photodissociation on a repulsive potential energy curve, are profoundly affected when this anion is embedded in a cluster of solvent atoms or molecules. Since charged clusters are readily mass-selected, one can in principle follow the evolution of this reaction with cluster size as the solute environment progresses from the gas phase to the condensed phase limits. Lineberger and coworkers first examined the anionic products of $Br_2^-(CO_2)_n$ photodissociation in 1988,[1] and subsequently expanded their scope to include I_2^- in CO_2, Ar, and OCS clusters, examining asymptotic products and time-resolved dynamics.[2–11] The experiments show that dissociation to ''uncaged'' I^- based products dominates for small clusters, while recombination to form ''caged'' I_2^- based products becomes competitive in clusters with a relatively small number of solvent molecules (less than one-half of a solvent shell). Experiments involving I_2^- photodissociation in numerous solvents have been pursued by Barbara and co-workers.[12–16] In solution, time scales for caging are similar to those of large $I_2^-(CO_2)_n$ clusters, although interesting new effects appear, such as the permanent escape of I^- into solution. Theoretical investigations of the structure and dynamics of I_2^- clusters have been performed by several groups.[17–30]

We have investigated $I_2^-(Ar)_n$ and $I_2^-(CO_2)_n$ clusters using femtosecond photoelectron spectroscopy (FPES).[31–33] In this experiment, mass-selected clusters are excited with a 780 nm femtosecond pump pulse from the $\tilde{X}(^2\Sigma_u^+)$ ground state to the $\tilde{A}'(^2\Pi_{g,1/2})$ dissociative state of I_2^- (Fig. 1). A second, delayed femtosecond probe pulse (260 nm) then detaches electrons from the clusters, producing a photoelectron spectrum. The FPE spectra provide a series of ''snapshots'' of the dynamics. In particular, one can track the evolution of the cluster through various electronic states and vibrational states, and also determine the number of solvent molecules adjacent to the negatively charged species (I_2^- or I^-) at any time.

Our most recent study on FPES of $I_2^-(Ar)_n$ clusters[33] demonstrated the effect of a weakly-interacting solvent on the I_2^- photodissociation reaction, such as closing of the dissociation channel through solvent-induced electronic transitions, dissipation of energy through solvent evaporation, and stabilization of an excited state. The $I_2^-(CO_2)_n$ system represents a stronger solute-solvent interaction than that of $I_2^-(Ar_2)_n$. While CO_2 lacks a dipole moment, its large quadrupole moment gives rise to a sizable $I_2^- \cdot CO_2$ well depth ($\sim$200 meV),[3] about four times larger than that of $I_2^- \cdot Ar$ (53 meV).[34] Solvent-induced effects seen in $I_2^-(Ar)_n$ clusters are therefore expected to be more pronounced in $I_2^-(CO_2)_n$ clusters. This paper reports on the use of FPES to investigate $I_2^-(CO_2)_n$ clusters, ranging in size from $n=4$, which produces almost exclusively uncaged $I^-(CO_2)_n$ fragments, to $n=16$, which yields only caged $I_2^-(CO_2)_n$ fragments.[3,6] The time scales for caging, vibrational relaxation and solvent rearrangement and evaporation are investigated as a function of cluster size.

The information obtained with FPES is complementary to previous experimental and theoretical work. Photofragment mass spectra of photodissociated $I_2^-(CO_2)_n$ clusters were measured by the Lineberger group at 720, 790, and 395 nm,[3,6,11] yielding complete product mass distributions and

[a]Current address: NASA Ames Research Center, Atmospheric Chemistry and Dynamics Branch, Mail Stop 245-5, Moffett Field, California 94035.

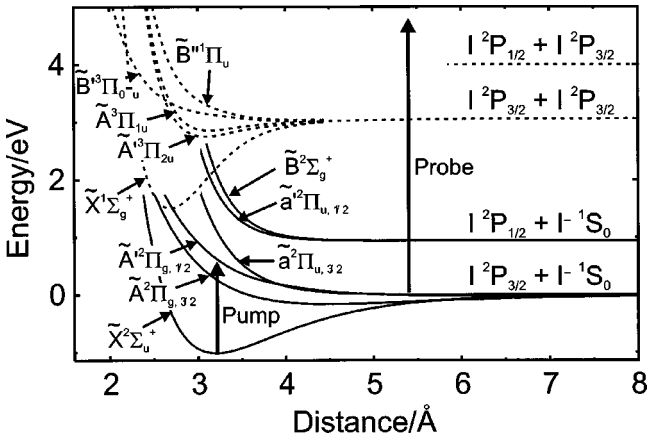

FIG. 1. Potential energy curves for bare I_2^-. Solid lines (—), I_2^-. Dotted lines (···), I_2.

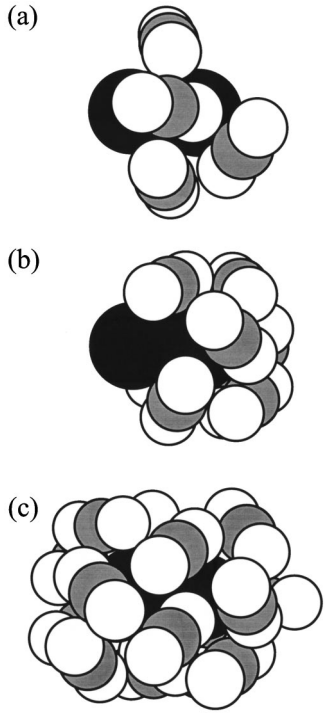

FIG. 2. Calculated minimum-energy structures (Refs. 20, 24, 35) of selected $I_2^-(CO_2)_n$ clusters: (a) $I_2^-(CO_2)_4$; (b) $I_2^-(CO_2)_9$; (c) $I_2^-(CO_2)_{16}$.

branching ratios for the caged and uncaged channels as a function of the number of solvent molecules. Time-resolved absorption recovery experiments on $I_2^-(CO_2)_n$ clusters were also performed by the Lineberger group. Here, mass-selected clusters were excited with a ps-duration laser pulse at 720 nm,[2–5] or a fs-duration pulse at 790 nm,[8] then re-excited with a second, identical pulse after a variable time delay. The observation of two-photon photofragments was taken as a signature of absorption of recombined I_2^- near the bottom of the $\tilde{X}$ state well. The risetime of this absorption yields the time scale for recombination and relaxation. The recovery time ($t_{1/e}=1.3-24$ ps) decreases with increasing cluster size, and in all cases is much faster than for $I_2^-(Ar)_{20}$ (127 ps).[8]

Theoretical work on $I_2^-(CO_2)_n$ clusters has focused on structure and dynamics. Minimum energy structures have been calculated by several groups and agree in large measure.[18,20,24,29] Figure 2 shows calculated structures for selected cluster sizes, taken from the Parson group.[20,24,35] The first three solvent molecules locate in a ring about the I_2^- internuclear axis. Additional molecules surround one I atom until no more space remains, after which the other I atom is solvated. A full shell is obtained for 16 solvent molecules. The charge is equally shared by both I atoms in the small and large clusters, but in the $n\approx 6-12$ size regime, where asymmetric structures are observed, the charge is more localized on the heavily solvated atom. This situation, termed ''normal charge-switching,''[20,23] applies to the I_2^- $\tilde{X}$ and $\tilde{A}$ states.

The mechanism of $I_2^-(CO_2)_n$ photodissociation has been investigated by Parson and co-workers[19,20,24,25,28,30] and Margulis and Coker[29] using nonadiabatic molecular dynamics (MD) simulations. Clusters ranging from 8 to 16 CO_2 molecules were considered. The simulations show that dissociation to well-separated I and I^- photofragments within the clusters occurs promptly, followed either by breakup of the cluster to form I and I^--based products, or recombination due to interactions with the solvent molecules that prevent photofragment escape. Both the extent and rate of recombination increase with cluster size in qualitative agreement with experiment.

There are many additional subtleties revealed by the simulations that are of interest. The simulations predict that the distribution of the excess charge on the I atoms plays an important role in the dynamics, particularly when the initial solvent geometry is highly asymmetric (i.e., $n\approx 6-12$). In these cases, excitation to the $\tilde{A}'$ state results in an energetically unfavorable solvent configuration, because the charge prefers to be localized on the less-solvated I atom; this effect is called ''anomalous charge-switching'' by Parson and co-workers.[20,23] The simulations thus predict rearrangement to a more symmetric solvent configuration on the $\tilde{A}'$ state, followed by non-adiabatic transitions to the $\tilde{A}$ and $\tilde{X}$ states. In clusters for which caging occurs, many of the trajectories pass through the $\tilde{A}$ state, where they are trapped for tens of picoseconds, en route to the $\tilde{X}$ state. Once the $\tilde{X}$ state is reached, vibrational relaxation occurs rapidly, in 3 ps or less,[24] and energy transfer to the solvent molecules results in their evaporation on a somewhat slower time scale. The simulations also indicate that the $\tilde{A}$ state is a ''solvent-separated'' state, with the I^- surrounded by most of the solvent molecules, and the I located outside the solvent shell, surrounded by fewer CO_2 molecules. One problem arising from the simulations is that the recovery time of the $\tilde{X}$ state absorption is slower than measured experimentally. This effect arises from the extensive trapping on the $\tilde{A}$ state in the simulations, which slows down the overall $\tilde{X}$ state recovery time.

FPES of $I_2^-(CO_2)_n$ clusters can in principle probe many of the effects predicted in the MD simulations. The results presented here therefore provide a detailed picture of dynamical trends across cluster size as well as clear points of comparison with theory. We find evidence for many of the MD predictions, including solvent reorganization related to anomalous charge-switching and the presence of a long-lived

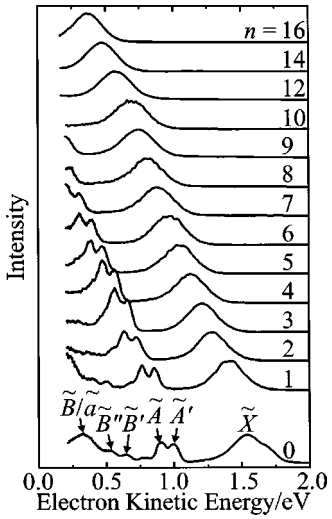

FIG. 3. One-photon photoelectron spectra of $I_2^-(CO_2)_n$ ($n=1-10$, 12, 14, 16) clusters. Photon energy=4.768 eV.

solvent-separated state. The observed time scales for vibrational relaxation on the ground state are compatible with the MD simulations. On the other hand, we find different dynamics on the $\tilde{A}$ state than predicted by the simulations which may serve to explain the discrepancies between the simulated and experimental absorption recovery times.

II. EXPERIMENT

The apparatus and data collection procedure is similar to that described previously.[33] $I_2^-(CO_2)_n$ clusters are produced by passing a mixture of 3% CO_2 in Ar at 20 psig over solid I_2 and expanding into vacuum through a pulsed piezoelectric valve. The pulsed jet is crossed by electrons from a 1.5 keV electron gun resulting in the production of negatively charged molecules and clusters. These anions are pulse-extracted into a Wiley–McLaren[36] time-of-flight mass spectrometer where they travel to the laser interaction region. Femtosecond pump (780 nm, 80 fs, 150 μJ) and probe (260 nm, 100 fs, 20 μJ) pulses generated from a Clark-MXR Ti:sapphire regeneratively amplified laser intersect the anions at the focus of a magnetic bottle electron spectrometer,[37] and photoelectrons produced are energy-analyzed by time-of-flight. The pulsed valve and laser operate at a repetition rate of 500 Hz.

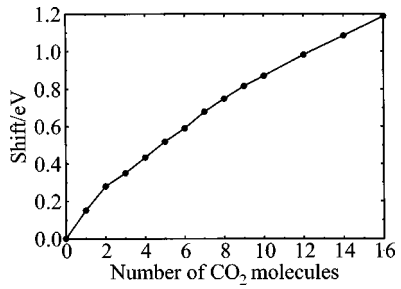

FIG. 4. Shift of the $\tilde{X}$ band in Fig. 3 vs n for $I_2^-(CO_2)_n$ clusters ($n=0-10$, 12, 14, 16).

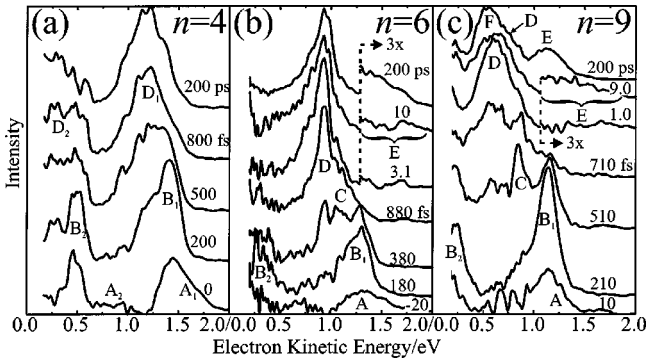

FIG. 5. FPE spectra of $I_2^-(CO_2)_n$ clusters at selected delay times: (a) $I_2^-(CO_2)_4$, (b) $I_2^-(CO_2)_6$, and (c) $I_2^-(CO_2)_9$. Pump photon energy = 1.589 eV, probe photon energy=4.768 eV.

To increase electron energy resolution, anions could be pulse-decelerated[38] just prior to laser interaction. Since this technique resulted in a loss of ~75% of the electron signal, it was only applied to clusters with relatively high anion flux [$I_2^-(CO_2)_n \leqslant 12$]. However, slowing down the heavier ions is less important due to their lower laboratory velocity. In general, the resolution for 1 eV electrons was 100–200 meV, depending on mass and conditions. Typical acquisition times were 80–1000 s per time delay. One-photon (probe only) photoelectron spectra of $I_2^-(CO_2)_n$ clusters ($n=1-10$, 12, 14, 16) were also collected, in order to determine the energy shift of I_2^- features due to the presence of CO_2 molecules. Acquisition times for these spectra were 1000–6000 s per cluster.

III. RESULTS

One-photon (probe only) photoelectron spectra of $I_2^-(CO_2)_n$ clusters ($n=0-10$, 12, 14, 16) are shown in Fig. 3. The spectra consist of transitions to various electronic states of I_2 as indicated in the $n=0$ spectrum. In all spectra, the peak at highest electron kinetic energy (eKE) results from photodetachment to the $\tilde{X}$ state of neutral $I_2(CO_2)_n$. The shift in the vertical detachment energy to this state relative to bare I_2^- (i.e., the shift in the peak center) is plotted vs n in Fig. 4. A monotonic shift toward lower electron kinetic energy is observed with increasing cluster size, ~150 meV per CO_2 molecule for $I_2^-(CO_2)$, and decreasing to ~50 meV/CO_2 for $I_2^-(CO_2)_{n\geqslant 10}$. These ''solvent shifts'' result from stronger solvent binding in the anion than in the neutral.[39]

Time-resolved photoelectron spectra for $I_2^-(CO_2)_n$ clusters with $n=4$, 6, 9, 12, 14, and 16 are shown in Figs. 5(a)–5(c) and 6(a)–6(c) for selected pump–probe delay times. Spectra were taken at many more delays than are shown in the figures; the selected spectra represent the minimum needed to follow the dynamics in these clusters. The spectra consist of peaks of various widths that evolve as a function of time. The maximum time delay recorded for each cluster is 200 ps.

Based on our recent detailed study of $I_2^-(Ar)_n$ (Ref. 33) and the mass spectroscopy studies of $I_2^-(CO_2)_n$ photofragmentation by Lineberger and co-workers,[6,7] many features in

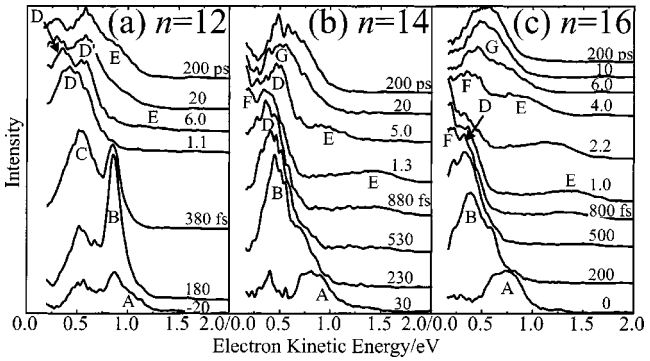

FIG. 6. FPE spectra of $I_2^-(CO_2)_n$ clusters at selected delay times; (a) $I_2^-(CO_2)_{12}$, (b) $I_2^-(CO_2)_{14}$, and (c) $I_2^-(CO_2)_{16}$. Pump photon energy=1.589 eV, probe photon energy=4.768 eV.

these spectra can be assigned at least on a preliminary basis. This assignment scheme is summarized in Table I. Feature A [A_1 and A_2 in Fig. 5(a)] seen at the earliest times, reflects the transient I_2^- created on the repulsive $\tilde{A}'$ state by the pump pulse; analysis of this feature has been reported elsewhere.[40]

Features B, C, and D are relatively sharp peaks that appear between 200 fs and 1.1 ps. We attribute these to photodetachment from solvated I^-. The subscripts 1 and 2, when shown ($n=4$, 6, 9) refer to photodetachment to the $^2P_{3/2}$ and $^2P_{1/2}$ states of atomic iodine, respectively. Since peaks B, C, and D occur at progressively lower eKE, they correspond to solvation by increasing numbers of CO_2 molecules. The progression in time and energy for these three features is most apparent for $I_2^-(CO_2)_6$, $I_2^-(CO_2)_9$, and $I_2^-(CO_2)_{12}$, where peak B is most intense at ~200 fs, peak C is most intense at ~400–500 fs, and peak D is most intense by ~800 fs–1.1 ps. A distinct feature C is not evident for the other clusters, but in all cases there is a net shift to lower electron energy from feature B at ~200 fs to feature D at ~800 fs–1.1 ps.

Feature E appears at high electron kinetic energy for all clusters except $I_2^-(CO_2)_4$. The earliest time at which it can be observed drops with increasing cluster size, from ~10 ps for $I_2^-(CO_2)_6$ to ~500 fs for $I_2^-(CO_2)_{14-16}$. Once this feature appears, it shifts toward lower electron kinetic energy with increasing time, and the degree of shifting is most apparent for the $I_2^-(CO_2)_{14-16}$ clusters. Based on our $I_2^-(Ar)_{20}$ results,[33] feature E at early times is attributed to photodetachment from the classical inner turning point region of a vibrationally excited I_2^- wavefunction resulting from recombination on the $\tilde{X}$ state. Subsequent shifting toward lower electron kinetic energy results from vibrational relaxation of the I_2^-. At time delays >5 ps for $n=14$ and >4 ps for $n=16$, feature E is relabeled feature G to signify that is has merged with lower energy features (see below). In clusters with $n \leqslant 12$, feature E remains distinguishable from other features in the spectrum at all time delays.

The trends at time delays beyond ~1 ps for $n=9$, 12, 14, and 16 clusters at low eKE ($\lesssim$1 eV) hint at more complex dynamics that were seen for $I_2^-(Ar)_n$ clusters. For $I_2^-(CO_2)_9$, the single feature D at 1.0 ps broadens slightly toward higher eKE at later times, and by 200 ps appears as a shoulder on the high energy side of a peak labeled F. For $I_2^-(CO_2)_{12}$, feature D splits into two features by 6.0 ps, D (at low eKE) and D′ (at high eKE), with feature E appearing as a shoulder on D′ at 200 ps. In the $I_2^-(CO_2)_{14}$ spectra, feature D begins shifting toward higher eKE after 1.3 ps, and merges with E by 20 ps, at which point the merged feature is labeled G. A low-energy feature, F, emerges after 880 fs. For $I_2^-(CO_2)_{16}$, D changes from a peak at 500 fs to a shoulder at 1.0 ps on a lower energy feature labeled F. By 4.0 ps, D is gone, leaving E and F, which merge into feature G by 6.0 ps.

Assignment of these features is possible only by comparison with simulations described below. These will demonstrate that peak F has a similar origin as in the $I_2^-(Ar)_n$ spectra, namely, photodetachment from the classical outer turning point of vibrationally excited I_2^- to the ground state of I_2, and from vibrationally relaxed I_2^- to the low-lying excited states of I_2. The simulations also suggest that the D features in clusters of $I_2^-(CO_2)_{n\geqslant 9}$ [and D′ in $I_2^-(CO_2)_{12}$] are at least partially due to long-lived, solvent-separated states of I_2^- within the cluster.

TABLE I. Labeling system of features observed in FPES of $I_2^-(Ar)_n$ and $I_2^-(CO_2)_n$ clusters, with corresponding assignments. In cases where two spin–orbit manifolds are visible (peaks A–D), each is labeled with a subscript, e.g., A_1 and A_2, according to decreasing eKE.

Label	Assignment
A	$I_2 \leftarrow I_2^- \tilde{X}$ (transient)
B	$I \leftarrow I^-$ (anomalous state)
C	$I \leftarrow I^-$ (symmetrically solvated)
D	$I \leftarrow I^-$ (dissociated), $I \leftarrow I^-$ (solvent-separated I_2^-)
E	$I_2\ \tilde{X} \leftarrow I_2^-\ \tilde{X}\ v \approx 0$, $I_2\ \tilde{X} \leftarrow I_2^-\ \tilde{X}$ excited inner turning point (ITP)
F	$I_2\ \tilde{X} \leftarrow I_2^-\ \tilde{X}$ excited outer turning point (OTP), I_2^* (higher-lying states) $\leftarrow I_2^-\ \tilde{X}$
G	$I_2\ \tilde{X} \leftarrow I_2^-\ \tilde{X}$ and $I \leftarrow I^-$ (indistinguishable)

IV. ANALYSIS

Simulations of the photoelectron spectra were performed in a manner similar to that for the $I_2^-(Ar)_n$ clusters,[33] using a combination of previously-measured photoelectron spectra to simulate the I^- features, and calculated photoelectron spectra to model vibrationally excited I_2^- features. Details of the methods used can be found in the previous paper,[33] and a discussion of the I_2 and I_2^- potential energy curves is given elsewhere.[40] The discussion below focuses on features of the analysis unique to the $I_2^-(CO_2)_n$ simulations.

Peaks B, C, and D are assigned to solvated I^-. The effective number of CO_2 molecules around the I^-, $\langle n_{I^-} \rangle$, was determined from previously-measured solvent shifts of $I^-(CO_2)_n$ clusters.[41–43] The shifts are much larger per CO_2 molecule than per Ar atom, ~170 meV for $I^-(CO_2)$, decreasing to ~40 meV for $I^-(CO_2)_{n\geqslant 10}$. The resulting value should correspond approximately to the instantaneous solvent coordination number of the I^- within the cluster.

For analysis of short-time ($\lesssim$1 ps) spectra, the eKE of features B, C, and D have been converted into $\langle n_{I^-} \rangle$ (using linear interpolation to calculate a fractional value when the eKE lay between measured shifts) and are presented in Table

TABLE II. Average number of solvent molecules coordinated to $I^-(\langle n_{I^-}\rangle)$ for features B, C, and D in $I_2^-(CO_2)_n$ clusters determined from the FPE spectra. Also given are estimates of $\langle n_{I^-}\rangle$ for anomalous ($\tilde{A}'$) and normal ($\tilde{X}$, $\tilde{A}$) charge-switching states derived from calculated cluster structures, and $\langle n_{I^-}\rangle$ for a symmetric solvent configuration on the $\tilde{A}'$ state (see text).[a]

Parent cluster	FPES			Model estimates		
	B	C	D	Anomalous	Symmetric	Normal
4	1.4	···	2.5	3.0	3.5	4.0
6	2.1	3.4	4.4	3.0	4.5	6.0
9	3.0	5.0	6.7	3.0	6.0	9.0
12	4.8	7.2	8.0	5.0	7.0	9.0
14	7.8	···	8.2	9.0	9.5	10.0
16	8.4	···	8.9	10.0	10.0	10.0

[a]Reference 24.

II. Also shown are estimates of $\langle n_{I^-}\rangle$ for the normal and anomalous charge-switching states, as defined in the Introduction. These latter values were obtained from calculated structures of the clusters,[24,28,35] assuming no change in solvent coordination number or loss of solvent during the first ps. Hence the ''normal'' and ''anomalous'' values of $\langle n_{I^-}\rangle$ represent the coordination numbers around the more and less highly solvated I atoms, respectively (compare to Fig. 2, for example). An estimate for a symmetrically-solvated structure is also given, obtained by averaging the anomalous and normal values. Table II is considered in more detail in the Discussion.

For simulating FPES spectra, actual $I^-(CO_2)_n$ photoelectron spectra were used,[42] rather than the shifted I^- spectra used for $I^-(Ar)_n$, because the $I^-(CO_2)_n$ spectra contain prominent progressions arising from CO_2 vibrational modes. Normalization of the spectra was achieved by scaling the integral of the $I\,^2P_{3/2}\leftarrow I^-\,^1S_0$ transition to that of the bare I^- spectrum [2.0, relative to 1.0 for the $I_2(\tilde{X})\leftarrow I_2^-(\tilde{X},v=0)$ transition].[33]

Solvated I_2^- in the $\tilde{X}(^2\Sigma_u^+)$ state was modeled using an empirically determined distribution of vibrational levels, characterized by an average level $\langle v\rangle$ and average number of solvent molecules $\langle n_X\rangle$. Given an I_2^- vibrational distribution, the method of generating a spectrum was the same as that used for $I_2^-(Ar)_n$ clusters;[33] appropriate solvent shifts of the simulated spectra were taken from the one-photon photoelectron spectra of $I_2^-(CO_2)_n$ clusters measured in this work (Fig. 4).

At long time delays, when $\langle v\rangle$ is fairly small ($\lesssim$5), $\langle n_X\rangle$ and $\langle v\rangle$ can be simultaneously determined from the spectrum by simulating feature E (or G). In this situation, the feature arises from an $I_2(\tilde{X})\leftarrow I_2^-(\tilde{X})$ band whose shape depends sensitively on $\langle v\rangle$, while the overall eKE of the band is governed by $\langle n_X\rangle$.

At larger $\langle v\rangle$, the $\tilde{X}\leftarrow\tilde{X}$ band splits into two distinct energy regions arising from different segments of the I_2^- vibrational wave function. Near the classical inner turning point (ITP) of the I_2^- potential, photodetachment results in a broad range of eKE, and the maximum eKE increases rapidly with $\langle v\rangle$. The $\tilde{X}\leftarrow\tilde{X}$ ITP contribution, lying at the highest eKE in the spectrum, corresponds to feature E at short time delays; however, as its eKE is dependent on $\langle n_X\rangle$ and $\langle v\rangle$, both quantities cannot be simultaneously determined from this feature.

Photodetachment near the classical outer turning point (OTP) to the I_2 ground state results in a much narrower and intense peak, occurring at lower eKE, and an even lower energy broad band from photodetachment to excited I_2 states (the $I_2^*\leftarrow\tilde{X}$ band). The eKE of the narrow peak is relatively insensitive to $\langle v\rangle$ over a wide range (~10–30), in principle allowing an independent determination of $\langle n_X\rangle$. While this method could be used in $I_2^-(Ar)_n$ clusters,[33] it generally cannot be applied to $I_2^-(CO_2)_n$ clusters, because the OTP transitions either are not accessible at the probe wavelength due to large solvent shifts, or they are masked by overlapping I^- features, making accurate determination of $\langle n_X\rangle$ difficult.

In such cases [time delays $\leqslant$30 ps for $I_2^-(CO_2)_{12}$, and somewhat shorter delays for $I_2^-(CO_2)_{14}$ and $I_2^-(CO_2)_{16}$], simulations using several values of $\langle n_X\rangle$ were performed. Several criteria were then considered in determining a ''best'' $\langle n_X\rangle$ time progression for the cluster. The value of $\langle n_X\rangle$ at long time delays, where it could be determined with more confidence, served as a primary constraint. It was assumed that $\langle n_X\rangle$ decreased monotonically with time delay, and that changes from one spectrum to another were not abrupt ($\leqslant$1 CO_2 molecule). The correspondence between the experimental spectra and simulations using different values of $\langle n_X\rangle$ was not equally good, further limiting the choices of $\langle n_X\rangle$. A final decision rested on careful comparison of $\langle n_X\rangle$ in neighboring clusters, and the average size distributions from the photofragmentation experiments at 790 nm.[3,6]

Populations of the I^- and I_2^- $\tilde{X}$ state contributions, P_{I^-} and P_X, respectively, were determined from the intensities of simulated spectral features, weighted by their relative cross sections. P_{I^-} and P_X sum to unity for all spectra. For clusters $I_2^-(CO_2)_{n\geqslant 9}$, it appears that some of the ''I^-'' signal is from the solvent-separated I_2^- structure (''SS I_2^-'') proposed by Parson[28] and Coker,[29] in which I_2^- is dissociated, with the I^- surrounded by solvent and the I atom still inside the cluster but separated by the I^- by at least one CO_2 molecule. This contribution is included in P_{I^-}.

Simulation parameters are summarized in a series of graphs in Figs. 7(a)–7(b) (P_X and $\langle v\rangle$ vs time) and ($\langle n_X\rangle$ and $\langle n_{I^-}\rangle$ vs time). Included in these figures are data from $I_2^-(Ar)_{20}$. Values of P_X, $\langle n_X\rangle$ and $\langle n_{I^-}\rangle$ at long times (~5 μs) obtained from Lineberger's photofragmentation experiments[3,6] are indicated as detached points. Although FPE spectra at several time delays have been simulated to follow the dynamics in each cluster, only a selected number are shown to illustrate the changes taking place. These are presented in Figs. 9(a)–9(f) ($n=6$, 9, and 12), 10(a)–10(c) ($n=14$), and 11(a)–11(d) ($n=16$). Each graph includes curves representing the solvated I^- and I_2^- $\tilde{X}$ contributions, the total simulated spectrum, and the experimental spectrum.

Estimated error bars are $\pm$15% for P_X and $\langle v\rangle$, and $\pm$0.5 for $\langle n_X\rangle$ and $\langle n_{I^-}\rangle$; these represent typical variations of the parameters within which good fits to the experimental spectra are obtained. Error bars for the $\tilde{X}$ state parameters are about 50% larger for $I_2^-(CO_2)_6$ at all times and $I_2^-(CO_2)_9$ at

early delay times ($\leqslant$10 ps), because feature E is of low intensity and spread out over a wide energy range in these spectra.

V. DISCUSSION

Cluster spectra are treated in three sections, grouped by similar dynamics; (1) $I_2^-(CO_2)_4$, which shows relatively simple solvated I^- formation, and no I_2^- formation, (2) $I_2^-(CO_2)_6$, $I_2^-(CO_2)_9$, and $I_2^-(CO_2)_{12}$, which exhibit more complex I^- dynamics, and increasing amounts of I_2^- recombination and vibrational relaxation, and (3) $I_2^-(CO_2)_{14}$ and $I_2^-(CO_2)_{16}$, for which the FPE spectra are dominated by rapid formation and relaxation of I_2^-. For reference, the fraction of I_2^- products measured in the photofragmentation experiments[6] are 0.03 in $I_2^-(CO_2)_4$, 0.29 in $I_2^-(CO_2)_6$, 0.70 in $I_2^-(CO_2)_9$, 0.85 in $I_2^-(CO_2)_{12}$, 0.95 in $I_2^-(CO_2)_{14}$, and 1.00 in $I_2^-(CO_2)_{16}$. Thus, there are essentially no I_2^--based photoproducts from $I_2^-(CO_2)_4$, and no I^--based products from $I_2^-(CO_2)_{14-16}$. After discussion of each group of clusters, trends across cluster size are summarized, and comparisons are made to previous experimental and theoretical work. Parallels with $I_2^-(Ar)_n$ clusters are also considered.

A. $I_2^-(CO_2)_4$

In $I_2^-(CO_2)_4$, I^--based products dominate in the photofragmentation experiments, and no I_2^- features are observed in the FPE spectra. This cluster is predicted to have a fairly symmetric initial solvent configuration, with three of the four solvent molecules around the I_2^- waist,[35] so the normal and anomalous coordination numbers in Table II differ by only one solvent molecule. With this cluster geometry, both photofragments can leave the cluster without significant interaction with a solvent molecule, hence the near total absence of caged product formation. Features B_1 and B_2, peaking at $\sim$200 fs, represent the earliest observable I^- signal, when the I^- and I are not very far apart and the system is presumably still on the $\tilde{A}'$ state. From 200 to 800 fs, these features shift and broaden toward lower eKE, and are relabeled D_1 and D_2 at 800 fs. No evolution of the spectra occurs after 800 fs. We find $\langle n_{I^-}\rangle = 1.4$ for B_1 at 200 fs, and $\langle n_{I^-}\rangle = 2.5$ for D_1 at 800 fs. Thus, the I^- photofragment is more heavily solvated at 800 fs than 200 fs, suggesting that the I^- initially pulls away from the cluster but does not escape because of its strong attraction to the CO_2 solvent molecules. Instead, as discussed previously in more detail,[32] the solvent molecules respond to this initial motion by ''following'' the I^- and it becomes more solvated by 800 fs. While this is occurring, the neutral I atom can leave the cluster more or less unhindered.

The $I_2^-(CO_2)_4$ dynamics at early times differ from those seen in $I_2^-(Ar)_6$, another cluster in which no caging occurs. There, the spectral feature associated with the I^- photofragment continuously shifts to *higher* eKE from 0.3 to 1.5 ps and then stops evolving, indicating that the I^- photofragment simply leaves the cluster, taking at most 1 Ar atom with it.[26,31,33] The difference between the two clusters is caused by the significantly stronger $I^-\cdot CO_2$ interaction which induces the solvent molecules to follow the I^- fragment.

Finally, we note that even at 200 ps, our value of $\langle n_{I^-}\rangle = 2.6$ is somewhat higher than observed by product mass analysis in the photofragmentation experiments[6] ($\langle n_{I^-}\rangle = 1.9$). This indicates that solvent evaporation from the $I^-(CO_2)_m$ fragments is incomplete at 200 ps.

B. $I_2^-(CO_2)_6$, $I_2^-(CO_2)_9$, and $I_2^-(CO_2)_{12}$

These intermediate-sized clusters exhibit both solvated I^- and I_2^- features in their spectra at long time delays, consistent with the photofragmentation experiments. They are also predicted[24,28,29,35] to have highly asymmetric initial solvent configurations, with the excess charge unequally distributed between the I atoms, and more solvent molecules surrounding the more negatively charged I atom.

Molecular dynamics (MD) simulations by Faeder *et al.*[26] on $I_2^-(CO_2)_{9,12}$ following excitation at 790 nm show that this asymmetry has a profound effect on the dissociation dynamics. Specifically, in the initial configuration of the excited $\tilde{A}'$ state, the more negatively charged I atom is *less* solvated because of anomalous charge-switching. It is therefore free to leave the cluster, but cannot because of its attraction to the solvent molecules. Instead, the simulations predict interactions between the I and I^- fragments are important at short times, leading to nonadiabatic transitions between the $\tilde{A}'$ state and lower-lying $\tilde{X}$ and $\tilde{A}$ states. These transitions are necessary not only for caging to occur, but also for dissociation since the neutral I atom is less solvated in the $\tilde{X}$ and $\tilde{A}$ states and can leave the cluster relatively easily. The configuration of the solvent molecules is strongly tied to the anion electronic state, with a symmetric configuration lowest in energy for the $\tilde{A}'$ state, and solvation of the more negatively charged I atom lower in energy for the normal charge-switching $\tilde{X}$ and $\tilde{A}$ states. Margulis and Coker[29] have performed MD simulations on $I_2^-(CO_2)_8$ at 720 nm excitation and find similar effects controlling the short-time dynamics.

1. Short-time dynamics

The evolution of peaks B, C, and D in the FPE spectra of these clusters during the first $\sim$1.0 ps can be interpreted in the context of the MD simulations. Table II shows that for all three clusters, $\langle n_{I^-}\rangle$ for feature B, the earliest ''solvated I^-'' feature, is closest to the anomalous value, meaning that the negative charge is initially on the less-solvated I atom in the $\tilde{A}'$ state and confirming the prediction of anomalous charge-switching in this state.

Between 200 fs–1.0 ps, feature B evolves into a transient feature C, which then evolves into a much longer-lived feature D; the three peaks occur at progressively lower eKE, indicating that $\langle n_{I^-}\rangle$ increases over this time interval as shown in Table II. Table II also shows a reasonable correspondence between the $\langle n_{I^-}\rangle$ values for features C and D and the expected $\langle n_{I^-}\rangle$ values for ''symmetric'' and ''normal'' configurations, respectively, of the solvent molecules. The experimental values are generally slightly lower, but this discrepancy could be attributed to evaporation of one CO_2 during the first $\sim$1 ps, or to large amplitude motion of the I atoms at early times.[28,29] In any case, this correspondence suggests that feature C corresponds to passing through a

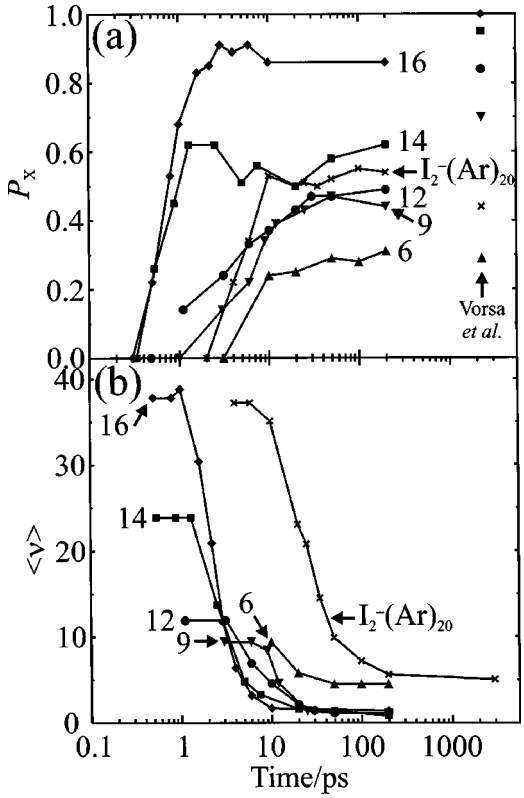

FIG. 7. Simulation parameters for $I_2^-(CO_2)_n$ clusters (a) Population of the I_2^- $\tilde{X}$ state (P_X) vs time. (b) Average vibrational level of the I_2^- $\tilde{X}$ state ($\langle v \rangle$) vs time. Legend, ▲$=I_2^-(CO_2)_6$, ▼$=I_2^-(CO_2)_9$, ●$=I_2^-(CO_2)_{12}$, ■ $=I_2^-(CO_2)_{14}$, ♦$=I_2^-(CO_2)_{16}$, ×$=I_2^-(Ar)_{20}$. Detached points indicate values from Vorsa *et al.* (Ref. 8).

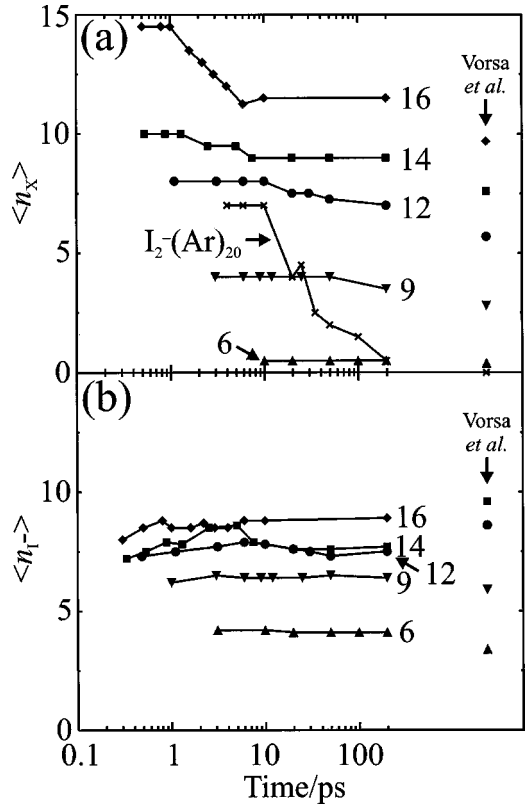

FIG. 8. Simulation parameters for $I_2^-(CO_2)_n$ clusters. (a) Average number of CO_2 molecules in the I_2^- $\tilde{X}$ state ($\langle n_X \rangle$) vs time. (b) Average number of CO_2 molecules solvating the I^- fragment ($\langle n_{I^-} \rangle$) vs time. Legend is identical to Fig. 7. Detached points indicate values from Vorsa *et al.* (Ref. 8).

symmetric solvent configuration, the lowest energy structure on the $\tilde{A}'$ state surface.[24] This symmetric geometry maximizes coupling with the lower-lying $\tilde{A}$ state, particularly at large interiodine separations where the two states are nearly degenerate. The evolution of peak C to peak D then suggests a nonadiabatic transition to a normal charge-switching state in which the I^- is preferentially solvated, i.e., either the $\tilde{A}$ or $\tilde{X}$ state, by 1 ps. Our interpretation of peaks B, C, and D is qualitatively consistent with the MD simulations by Faeder *et al.*,[28] which predict that the solvent rearranges to a symmetric configuration within 500 fs, followed by transitions to the $\tilde{A}$ or $\tilde{X}$ states at later time delays.

Note that feature D can in general result from a true $I^-(CO_2)_n$ cluster (from which the I atom has departed), or a cluster in which I and I^- are both present but far apart; the two are difficult to distinguish spectroscopically because of the relatively weak I-CO_2 interaction[41] (45 meV well depth). This point is important because recombination can occur with nonzero probability as long as both atoms are present in the cluster.

2. Longer-time dynamics

a. $I_2^-(CO_2)_6$: The $I_2^-(CO_2)_6$ spectra were simulated between 3–200 ps. The full set of simulation parameters is shown in Figs. 7 and 8. Figure 7(a) shows that 10 ps is the earliest time at which $P_X > 0$. P_X grows from 0.24 at 10 ps to 0.31 at 200 ps [Fig. 7(a)], while $\langle v \rangle$ decreases in step with the rise of P_X [Fig. 7(b)] from 9.4 to 4.5; $\langle n_X \rangle$ and $\langle n_{I^-} \rangle$ are essentially constant at 0.5 and 4, respectively, from 10 to 200 ps [Figs. 7(a)–7(b)].

It therefore appears that between 3 and 10 ps, the earliest time at which a discernible feature E can be seen, substantial recombination, relaxation, and solvent evaporation has occurred; the I_2^- chromophore has dissipated about 870 meV of vibrational energy (out of a total well depth of ~1 eV), and most of the solvent molecules have evaporated. Presumably the $\tilde{X}$ state vibrational distribution is too spread out and the population of this state too low for feature E to be observable before 10 ps. After 10 ps, additional recombination occurs along with a small amount of vibrational relaxation. In contrast to the larger clusters, $I_2^-(CO_2)_6$ loses all its solvent molecules before complete relaxation can occur, so that $\langle v \rangle$ at 200 ps is higher than for any other cluster studied here [see Fig. 7(b)].

Since relatively minor changes occur after 10 ps, only the 200 ps simulation is shown [Fig. 9(a)]. The simulation parameters ($P_X = 0.31$, $\langle v \rangle = 4.5$, $\langle n_X \rangle = 0.5$, $\langle n_{I^-} \rangle = 4.1$) indicate a spectrum dominated by solvated I^-, which accounts for almost all of feature D. Solvated $I_2^-(\tilde{X})$ contributes a fairly uniform, low-intensity signal over the entire range of observed electron kinetic energies, 0–2 eV, with a distinctive, sloping shape in the region of the E feature, arising from the $\tilde{X} \leftarrow \tilde{X}$ transition, and a slight increase at 750 meV due to the $\tilde{A}'/\tilde{A} \leftarrow \tilde{X}$ transitions. The photofragmentation

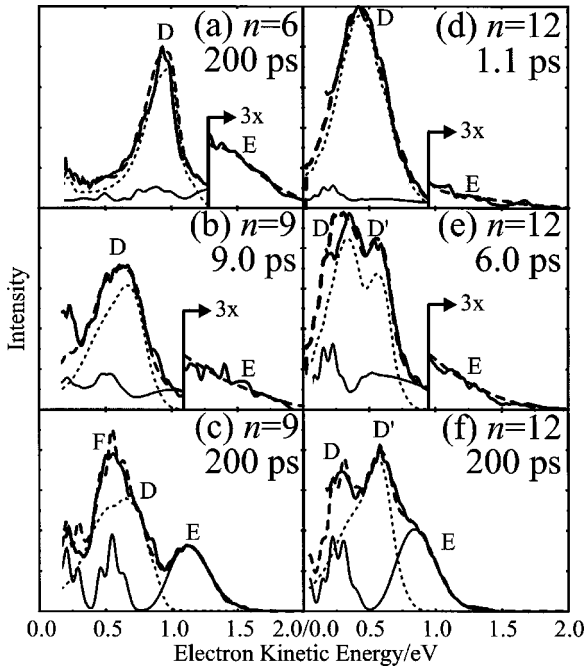

FIG. 9. Experimental (thick solid) and simulated (dashed) spectra of (a) $I_2^-(CO_2)_6$ at 200 ps, (b) $I_2^-(CO_2)_9$ at 9.0 ps, (c) $I_2^-(CO_2)_9$ at 200 ps, (d) $I_2^-(CO_2)_{12}$ at 1.1 ps, (e) $I_2^-(CO_2)_{12}$ at 6.0 ps, and (f) $I_2^-(CO_2)_{12}$ at 200 ps. Contributions to simulated spectra from the I_2^- $\tilde{X}$ state (thin solid) and solvated I^- (dotted) are also shown. The I^- contribution includes the solvent-separated state (see text).

experiments[6] yielded $\langle n_X\rangle = 0.4$, in good agreement with our value. However, as was the case for $I_2^-(CO_2)_4$, our value of $\langle n_{I^-}\rangle$ at 200 ps is larger than the photofragmentation value (3.4), which points to vibrational excitation and incomplete evaporation in the solvated I^- fragment at 200 ps.

b. $I_2^-(CO_2)_9$: The FPE spectra of $I_2^-(CO_2)_9$ were simulated from 1.0 to 200 ps. More significant changes in the shape of feature E are observed than in $I_2^-(CO_2)_6$, so two time delays (9.0 and 200 ps are shown in Figs. 9(b)–9(c) to illustrate the changes. The 9.0 ps spectrum ($P_X = 0.34$, $\langle v\rangle = 8.4$, $\langle n_X\rangle = 4.0$, $\langle n_{I^-}\rangle = 6.4$) shows an $\tilde{X}$ state contribution similar to that for $I_2^-(CO_2)_6$ in Fig. 9(a). Feature D is almost entirely accounted for by solvated I^-. In contrast, the 200 ps spectrum ($P_X = 0.44$, $\langle v\rangle = 1.1$, $\langle n_X\rangle = 3.5$, $\langle n_{I^-}\rangle = 6.4$) exhibits a much more structured $\tilde{X}$ state contribution due to the low average vibrational quantum number, with distinct peaks at 1.15 eV ($\tilde{X} \leftarrow \tilde{X}$, feature E), ~550 meV ($\tilde{A}'/\tilde{A} \leftarrow \tilde{X}$, feature F), and ~250 meV ($\tilde{B}'/\tilde{B}'' \leftarrow \tilde{X}$). Solvated I^- still accounts for the majority of the intensity of D; it is broadened and diminished relative to 9.0 ps, but otherwise unchanged.

P_X [Fig. 7(a)] is first observed to be nonzero at 3 ps, earlier than in $I_2^-(CO_2)_6$, and remains essentially constant (~0.44) after 25 ps. $\langle v\rangle$ [Fig. 7(b)] falls as P_X rises, dropping from 9.4 at 3 ps to 1.4 by 25 ps, after which there is little change. We find $\langle n_X\rangle = 4$ at all time delays $\geqslant 3$ ps until 200 ps, when it drops to 3.5, while $\langle n_{I^-}\rangle$ is constant (at 6.4) from 1 to 200 ps. The values of $\langle v\rangle$ and $\langle n_X\rangle$ at 3 ps indicate that significant recombination with associated dynamics has already occurred by the time feature E can be discerned, as was also the case for $I_2^-(CO_2)_6$. Subsequent vibrational relaxation is faster and more complete in $I_2^-(CO_2)_9$, reflecting the larger number of solvent molecules. However, while considerable vibrational relaxation occurs between 3 and 25 ps, the number of solvent molecules is unchanged, and at 200 ps, both $\langle n_X\rangle$ and $\langle n_{I^-}\rangle$ are slightly larger the photofragmentation averages[6] of 2.8 and 5.9, respectively. Thus, there is clearly a delay between the transfer of energy to the solvent and the evaporation of solvent molecules, a trend seen in the larger clusters as well.

At 200 ps, $P_X = 0.44$ is far smaller than the photofragmentation value of 0.70. This apparent discrepancy is explained by postulating that approximately half of the I_2^- population is trapped in a solvent-separated (SS) I_2^- structure, in which both I and I^- lie within the cluster but are separated by one CO_2 molecule; in our experiment these states should appear as solvated I^-. Long-lived SS I_2^- states are seen in the simulations of Faeder[28] and Margulis,[29] and are attributed to recombination on the I_2^- $\tilde{A}$ state, for which the well depth (~100 meV) is about half the $I^-\cdot CO_2$ well depth. However, the SS states in the simulations are predicted to decay on a time scale of tens of picoseconds, whereas our analysis of the $I_2^-(CO_2)_9$ FPE spectra indicates this state lasts at least 200 ps. We consider the SS states in more detail below in the context of results for $I_2^-(CO_2)_{12}$ clusters.

c. $I_2^-(CO_2)_{12}$: $I_2^-(CO_2)_{12}$ clusters were simulated from 1.1 to 200 ps, with the simulation parameters plotted in Figs. 7 and 8. The spectra exhibit significant changes during this time interval; three simulation examples (1.1, 6.0, and 200 ps) are shown in Figs. 9(d)–9(f). At 1.1 ps, the spectrum ($P_X = 0.14$, $\langle v\rangle = 11.9$, $\langle n_X\rangle = 8.0$, $\langle n_{I^-}\rangle = 7.5$) is almost entirely due to solvated I^-; the contribution from solvated $I_2^-(\tilde{X})$ accounts for the weak feature E at high eKE, and a small amount of intensity underlying feature D. The spectrum at 6.0 ps ($P_X = 0.33$, $\langle v\rangle = 6.9$, $\langle n_X\rangle = 8.0$, $\langle n_{I^-}\rangle = 7.9$) has a considerably larger contribution from $I_2^-(\tilde{X})$, resembling that for $I_2^-(CO_2)_9$ at 9.0 ps, with $E(\tilde{X} \leftarrow \tilde{X})$ appearing as a sloped feature, and increased intensity at ~200 meV ($\tilde{A}'/\tilde{A} \leftarrow \tilde{X}$). In addition, the single peak D seen at 1.1 ps has split into two peaks, D and D′. Most of D and all of D′ are fit using a bimodal $I^-(CO_2)_m$ distribution with maxima at $m = 9$ (D) and $m = 7$ (D′); the remainder of D is from the $\tilde{A}'/\tilde{A} \leftarrow \tilde{X}$ transition. The 200 ps spectrum ($P_X = 0.49$, $\langle v\rangle = 1.1$, $\langle n_X\rangle = 7.0$, $\langle n_{I^-}\rangle = 7.5$) exhibits strong $I_2^-(\tilde{X})$ state contributions centered at 850 meV ($\tilde{X} \leftarrow \tilde{X}$, feature E) and ~200 meV ($\tilde{A}'/\tilde{A} \leftarrow \tilde{X}$, accounting for half the intensity of feature D). The I^- contribution is bimodal but much less double-peaked than at 6 ps; the $m = 9$ component that contributes to D is considerably smaller than the $m = 7$ component comprising all of feature D′.

The drop in the $I^-(CO_2)_m$ contribution to peak D occurs primarily between 6 and 20 ps and is accompanied by an increase in P_X from 0.33 to 0.43. During this interval recombination of I and I^- within the cluster must be occurring. The time scale over which this process occurs is similar to the overall recovery time (~10 ps) of the I_2^- absorption seen by Lineberger[8] for clusters in this size range. By 200 ps, the remaining I^- contribution to peak D is attributed to true

$I^-(CO_2)_m$ fragments; this is consistent with the results of Vorsa *et al.*,[6,8] who found an $I^-(CO_2)_m$ fragment distribution from $I_2^-(CO_2)_{12}$ with average $m=8.6$ and no photofragments with $m<8$.

The largest feature in the FPE spectrum at 200 ps is peak D′, another I^- feature, in apparent disagreement with the photofragmentation results which yield a caging fraction of 0.85. Our value of P_X, 0.47, is considerably lower than this. We attribute peak D′ to solvent-separated I_2^-; assuming that all of the SS I_2^- eventually recombines (i.e., long after 200 ps) on the $\tilde{X}$ state, P_X may be added to the SS I_2^- population to obtain a caging fraction of 0.87, very close to the photofragmentation value. The situation is similar to that proposed for $I_2^-(CO_2)_9$, but the presence of a distinct peak D′ for the $n=12$ cluster at 200 ps provides a more compelling reason to make such an assignment.

Our value of $\langle n_{I^-}\rangle = 7.3$–$7.9$ for peak D′ between 6–200 ps is almost certainly less than the number of CO_2 molecules in clusters with long-lived SS I_2^- structures, because the formation of such a structure should not liberate enough energy to evaporate 5 CO_2 molecules (at 200 ps, $\langle n_X\rangle = 7.0$ for fully vibrationally-relaxed I_2^-). This suggests that in the long-lived SS I_2^- structure, some CO_2 molecules either surround the neutral I atom, or interact with the I^- atom more weakly than in a pure $I^-(CO_2)_n$ cluster.

C. $I_2^-(CO_2)_{14}$ and $I_2^-(CO_2)_{16}$

At short delay times, the $I_2^-(CO_2)_{14}$ and $I_2^-(CO_2)_{16}$ FPE spectra show feature A, associated with dissociating I_2^-, evolving into a solvated I^- feature B by 200 fs. This then shifts to slightly lower eKE (feature D) by 800–900 fs indicating increased solvation; the shift is more evident for $I_2^-(CO_2)_{14}$. Table II shows that the shift from B to D is noticeably smaller than for the $n=6$, 9, and 12 clusters. It is likely that the early time dynamics involving nonadiabatic transitions are similar for all five clusters, but that the energetic shifts associated with these transitions are smaller for the $n=14$ and 16 clusters because they start from more symmetric solvent configurations.

The distinguishing feature of these FPE spectra, however, is the early appearance of feature E (~500 fs) and the clear evolution of this feature toward lower eKE at later times. These trends result from the formation of solvated, highly vibrationally excited I_2^- and its subsequent relaxation, and allow us to follow the dynamics within these clusters in more detail than for the smaller clusters.

Simulations of the $I_2^-(CO_2)_{14}$ spectra at three time delays are shown in Figs. 10(a)–10(c) for 1.3, 5.0, and 200 ps. The 1.3 ps spectrum ($P_X=0.62$, $\langle v\rangle = 23.9$, $\langle n_X\rangle = 10.0$, $\langle n_{I^-}\rangle = 7.8$) exhibits a solvated I_2^- $\tilde{X}$ state spectrum which is very extended, due to the large value of $\langle v\rangle$; feature E is accounted for by the $\tilde{X}\leftarrow\tilde{X}$ ITP transition at high eKE, while F is represented at very low eKE by a combination of $\tilde{X}\leftarrow\tilde{X}$ OTP and $I_2^*\leftarrow\tilde{X}$ transitions (defined in the Analysis). Solvated I^- contributes the bulk of the intensity to D. In the 5.0 ps spectrum ($P_X=0.51$, $\langle v\rangle = 4.4$, $\langle n_X\rangle = 9.0$, $\langle n_{I^-}\rangle = 8.3$), $\langle v\rangle$ is much lower, generating a more compact $\tilde{X}\leftarrow\tilde{X}$ feature which accounts for feature E at much lower eKE, and part of D; the $\tilde{A}'/\tilde{A}\leftarrow\tilde{X}$ transition accounts for F. The solvated I^- contribution peaks at ~300 meV, between D and F, but represents about 2/3 of the intensity of D. The 200 ps spectrum ($P_X=0.62$, $\langle v\rangle = 0.8$, $\langle n_X\rangle = 9.0$, $\langle n_{I^-}\rangle = 7.7$) consists of a single broad feature G, which is accounted for roughly equally by solvated $I_2^-(\tilde{X})$, centered at high eKE and an I^- feature centered at lower eKE.

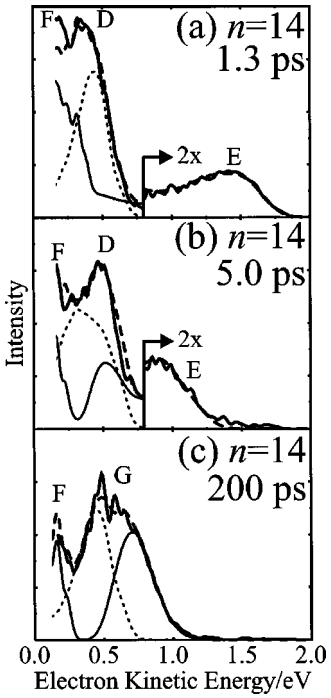

FIG. 10. Experimental (thick solid) and simulated (dashed) spectra of $I_2^-(CO_2)_{14}$ at (a) 1.3 ps, (b) 5.0 ps, (c) 200 ps. Contributions to simulated spectra from I_2^- $\tilde{X}$ state (thin solid) and solvated I^- (dotted) are also shown. The I^- contribution includes the solvent-separated state (see text).

Experimental and simulated FPE spectra of $I_2^-(CO_2)_{16}$ are shown in Figs. 11(a)–11(d) at 1.0 ps, 2.2 ps, 4.0 ps, and 200 ps. At 1.0 ps ($P_X=0.68$, $\langle v\rangle = 38.8$, $\langle n_X\rangle = 14.5$, $\langle n_{I^-}\rangle$

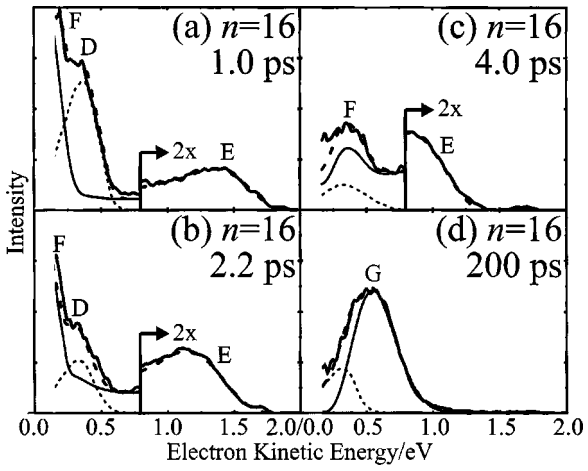

FIG. 11. Experimental (thick solid) and simulated (dashed) spectra of $I_2^-(CO_2)_{16}$ at (a) 1.0 ps, (b) 2.2 ps, (c) 4.0 ps, (d) 200 ps. Contributions to simulated spectra from the I_2^- $\tilde{X}$ state (thin solid) and solvated I^- (dotted) are also shown. The I^- contribution includes the solvent-separated state (see text).

$=8.5$), solvated I_2^- $\tilde{X}$ is responsible for features E ($\tilde{X}\leftarrow\tilde{X}$ ITP) and F ($\tilde{X}\leftarrow\tilde{X}$ OTP), while solvated I^- accounts for D. The very intense feature F is due to the much larger value of $\langle v\rangle$ in comparison to $I_2^-(CO_2)_{14}$ near this time delay. Also in contrast to $I_2^-(CO_2)_{14}$, the $\tilde{A}'/\tilde{A}\leftarrow\tilde{X}$ transitions are inaccessible at the probe wavelength because of the larger solvent shift. By 2.2 ps ($P_X=0.85$, $\langle v\rangle=20.9$, $\langle n_X\rangle=13.0$, $\langle n_{I^-}\rangle=8.7$), the general shape of the spectrum is unchanged, but E has moved to much lower eKE, and the intensity of F is diminished, due to the considerable $\tilde{X}$ state relaxation and loss of CO_2 molecules compared with 1.0 ps. The $\tilde{X}$ state population has increased significantly as well. The solvated I^- contribution, still accounting for D, is of lower intensity but $\langle n_{I^-}\rangle$ is almost identical. The 4.0 ps spectrum ($P_X=0.89$, $\langle v\rangle=6.4$, $\langle n_X\rangle=12.0$, $\langle n_{I^-}\rangle=8.5$) could be simulated exclusively by the I_2^- $\tilde{X}$ state, but there is better reproduction of the low eKE region if a small amount of I^- is included in the vicinity of F. The 200 ps spectrum ($P_X=0.86$, $\langle v\rangle=1.4$, $\langle n_X\rangle=11.5$, $\langle n_{I^-}\rangle=8.9$) reveals further vibrational relaxation to the $\tilde{X}$ state, and whether any I^- is present depends primarily on the choice of $\langle n_X\rangle$; over the range $\langle n_X\rangle=10.5-12.0$, P_X varies from 0.70 to 1.00. Here we choose a median value, which is most consistent with simulations at earlier time delays. The $\tilde{X}\leftarrow\tilde{X}$ transition accounts for the majority of G, with the solvated I^- signal making a small contribution to the low eKE side.

The trends in P_X and $\langle v\rangle$ in Fig. 7 are similar for $I_2^-(CO_2)_{14}$ and $I_2^-(CO_2)_{16}$. In both cases, P_X rises much more quickly than for the smaller clusters, reaching a plateau by 1.3 ps and 2.2 ps for the $n=14$ and 16 clusters, respectively. The initial value of $\langle v\rangle$ is much higher for these clusters, 24 ($n=14$) and 39 ($n=16$), then drops rapidly after 1 ps with nearly all vibrational relaxation occurring by 10 ps. These trends indicate a substantially higher rate of recombination vs. vibrational relaxation as compared to the smaller clusters. Figure 8(a) shows considerable solvent evaporation from the X state between 1 and 10 ps, particularly for $I_2^-(CO_2)_{16}$. This is the same time interval over which most of the vibrational relaxation occurs, indicating a strong correlation between vibrational relaxation and solvent evaporation. However, in both cases the 200 ps value of $\langle n_X\rangle$ is larger (by 1.5–1.8) than the photofragmentation average, reflecting the energy residing in the cluster which will eventually dissipate through CO_2 evaporation.

There is significant leeway in the choice of parameters for simulating the 200 ps spectrum for $I_2^-(CO_2)_{14}$, but the breadth of feature G in comparison to the $I_2^-(CO_2)_{16}$ spectrum suggests the presence of a significant I^- component, comparable to earlier time delays. P_X at 200 ps (0.62) is much smaller than observed in the photofragmentation experiments (0.95), and $\langle n_{I^-}\rangle$ is also significantly smaller (7.7 vs. 9.6). We therefore attribute this I^- component to long-lived, solvent-separated I_2^-, just as for $I_2^-(CO_2)_{9,12}$. There also appears to be a similar but smaller long-lived I^- contribution persisting through 200 ps in the $I_2^-(CO_2)_{16}$ spectra. This too is attributed to long-lived SS I_2^-, because I^- products were not observed in the photofragmentation experiments.

D. Trends across cluster size, and comparisons with other studies

The most significant trend across cluster size is the increasingly rapid appearance and subsequent vibrational relaxation of the I_2^- $\tilde{X}$ state. Using the time of initial appearance of feature E ($\tilde{X}\leftarrow\tilde{X}$ transition) as a basis of comparison [see Fig. 7(a)], a monotonic decrease with cluster size is observed, from $\sim$10 ps in $I_2^-(CO_2)_6$ to $\sim$500 fs in $I_2^-(CO_2)_{14-16}$, indicating that the recombination rate increases markedly with cluster size. This trend is presumably due to the increasing perturbation on the I_2^- electronic states by larger numbers of CO_2 molecules, facilitating nonadiabatic electronic transitions to the $\tilde{X}$ state. We also find that the initial value of $\langle v\rangle$ increases substantially with cluster size [Fig. 7(b)], from 9.4 for $I_2^-(CO_2)_6$ to 39 for $I_2^-(CO_2)_{16}$. This suggests that for the smaller clusters, vibrational relaxation in high vibrational levels of the I_2^- manifold is fast relative to the recombination rate, so significant relaxation has already occurred that by the time P_X is large enough (0.15–0.25) to produce an observable feature E. The higher initial $\langle v\rangle$ for the larger clusters reflects the increased recombination rate relative to vibrational relaxation.

In all clusters, we observe a buildup of population in the $\tilde{X}$ state to nearly its maximum value (i.e., at 200 ps) followed by vibrational relaxation. The time scale for this buildup is about 10 ps for $I_2^-(CO_2)_6$, $I_2^-(CO_2)_9$, and $I_2^-(CO_2)_{12}$, and about 1 ps for $I_2^-(CO_2)_{14}$ and $I_2^-(CO_2)_{16}$. Once there is substantial population in the $\tilde{X}$ state, vibrational relaxation proceeds more rapidly in the larger clusters. Although not directly comparable to our determinations of P_X and $\langle v\rangle$, the absorption recovery experiments of Vorsa *et al.*[8] confirm the general decrease in time required to reach a low vibrational state, with exponential time constants (at 790 nm excitation) ranging from 24 ps for $I_2^-(CO_2)_6$ to 1.3 ps for $I_2^-(CO_2)_{16}$. These time constants correspond approximately to the time at which $\langle v\rangle$ crosses $\sim$7 in Fig. 7(b). The rapid vibrational relaxation we observe in $I_2^-(CO_2)_{14}$ and $I_2^-(CO_2)_{16}$ is also in good agreement with the simulations, which predict that vibrational relaxation is very fast (1–3 ps) once a transition to the $\tilde{X}$ state occurs. In general, vibrational relaxation is much more rapid in $I_2^-(CO_2)_n$ than in $I_2^-(Ar)_n$, in agreement with Vorsa's results;[8] the FPES simulation parameters for $I_2^-(Ar)_{20}$ are shown in Figs. 7 and 8 for comparison.

Comparison of our values of $\langle n_X\rangle$ and $\langle n_{I^-}\rangle$ at 200 ps with the photofragmentation studies at 790 nm shows evaporation of solvent molecules is incomplete by 200 ps. For caged photoproducts, this effect is clear for all clusters with $n\geqslant 9$; the deviation is largest for $n=16$. For these clusters, vibrational relaxation within the $\tilde{X}$ state is complete by 25 ps or less. There is therefore a substantial delay between energy transfer to the solvent molecules and their evaporation. This effect was seen to a much lesser extent in $I_2^-(Ar)_{20}$ [Figs. 7(b) and 8(a)]; the longer hysteresis for the $I_2(CO_2)_n$ clusters is presumably due to stronger solvent binding and low frequency bending vibrations that greatly increase the density of vibrational levels.

The FPE spectra for $n\geqslant 9$ clusters all show evidence for solvent-separated structures. Comparison of the $\tilde{X}$ state

populations with the cage fractions in the photofragmentation experiments provides strong evidence for solvent-separated states with lifetimes exceeding 200 ps for these clusters, particularly the $n=9$, 12, and 14 clusters. MD simulations[28,29] attribute SS I_2^- states to metastable recombination on the $\tilde{A}$ state. However, our finding of a very long-lived state is at odds with the simulations which decay by recombination or dissociation on a time scale of tens of picoseconds. It is therefore useful to compare our conclusions regarding these states with previous experiments.

The photofragment mass spectra for $I_2^-(Ar)_n$ clusters show a bimodal $I_2^-(Ar)_m$ daughter ion distribution.[7] This is now attributed to metastable recombination on the $\tilde{A}$ state with a lifetime of at least 5 μs, the time scale of the experiment; in clusters where this occurs, the number of solvent molecules is considerably larger because of energy tied up as I_2^- electronic excitation. A bimodal mass distribution is *not* seen for $I_2^-(CO_2)_n$ photofragments,[3,5] implying that any long-lived states must decay by 5 μs. Our observation of a state lasting for at least 200 ps is certainly not in conflict with the mass spectrometry results; the more significant solvent-induced perturbations in $I_2^-(CO_2)_n$ clusters are likely to reduce the lifetime of any metastable or solvent-separated excited states than in $I_2^-(Ar)_n$ clusters.

The proposed long-lived solvent-separated state might seem at first to contradict Lineberger's observation of a short recovery time (1.3 ps) for $I_2^-(CO_2)_{16}$ at 790 nm excitation.[3,5] We also see $\tilde{X}$ state formation and vibrational relaxation on this time scale. In both experiments, this short-time signal must be from clusters which do not pass through the solvent-separated state en route to the $\tilde{X}$ state. Relaxation from the $\tilde{A}$ state with a lifetime greater than 200 ps would not contribute to either experiment, since delay times above 200 ps were not examined. As mentioned in the Introduction, one of the problems in comparing the MD simulations with Lineberger's experiments is that the predicted absorption recovery time for $I_2^-(CO_2)_{16}$ is too long, because part of the signal contributing to this recovery time comes from ions trapped for tens of picoseconds on the $\tilde{A}$ state.[28,29] A longer-lived solvent separated state resolves this discrepancy, since it would not contribute to the absorption recovery on the time scale of the simulations.

Overall, issues regarding recombination on the $\tilde{A}$ state represent the most significant area of contention between experiment and the simulations, not a surprising result since this state is poorly characterized, and nonadiabatic transitions involving this state are brought about by relatively weak interactions at large interiodine distances. Experiments to spectroscopically characterize the $\tilde{A}$ state are currently underway in our laboratories.

VI. CONCLUSIONS

The time-resolved photodissociation dynamics of $I_2^-(CO_2)_n$ clusters have been investigated using FPES for a range of sizes covering the uncaged and fully-caged product limits. In all clusters, solvated I^- is produced on the anomalous charge-switching $\tilde{A}'\,^2\Pi_{1/2,g}$ state in ~200 fs. This fragment becomes more solvated by ~800 fs–1.1 ps through a combination of solvent rearrangement and electronic transitions to the normal charge-switching $\tilde{A}$ and/or $\tilde{X}$ states.

In $I_2^-(CO_2)_{n\geqslant 6}$ clusters, the transition to the $\tilde{X}/\tilde{A}$ state induces I_2^- recombination, the fraction of which increases with cluster size. For $I_2^-(CO_2)_{n\leqslant 12}$, $\langle v\rangle = 9-12$ at the earliest time that recombination is observed. By 200 ps, we find $\langle v\rangle = 5$ for $I_2^-(CO_2)_6$, and $\langle v\rangle = 1$ for $I_2^-(CO_2)_{9,12}$. In $I_2^-(CO_2)_{14-16}$, recombination occurs much faster, and higher initial values of $\langle v\rangle$ are observed (up to ~40). The overall rate of vibrational relaxation increases dramatically from $I_2^-(CO_2)_6$ to $I_2^-(CO_2)_{16}$.

The numbers of solvent molecules around I^- and I_2^- products at 200 ps are larger than those observed in the photofragmentation experiments, implying that evaporation of CO_2 from the cluster occurs on a much longer time scale. This is consistent with the assumption that the CO_2 cage stores a considerable amount of energy in vibrational and/or cluster modes after removing it from I^- kinetic energy or I_2^- vibration. The discrepancy increases with cluster size, illustrating the increasing energy ''storage capacity'' of larger clusters.

In clusters of $I_2^-(CO_2)_{n\geqslant 9}$, a solvent-separated I_2^- structure is observed at long time delays, appearing spectroscopically as solvated I^-. This structure is needed to explain the high intensity of I^- features observed in these spectra, and the small number of CO_2 molecules surrounding I^-. While the lifetime of this metastable state appears to be >200 ps (the longest time delays measured), it is less than 5 μs the time scale of the photofragment mass spectrometry experiments.

ACKNOWLEDGMENTS

Research support from the National Science Foundation under Grant No. CHE-9710243 and from the Defense University Research Instrumentation Program under Grant No. F49620-95-1-0078, are gratefully acknowledged. The authors would like to thank James Faeder, Nicole Delaney, and Professor Robert Parson at the University of Colorado, Boulder for many helpful discussions.

[1] M. L. Alexander, N. E. Levinger, M. A. Johnson, D. Ray, and W. C. Lineberger, J. Chem. Phys. **88**, 6200 (1988).
[2] D. Ray, N. E. Levinger, J. M. Papanikolas, and W. C. Lineberger, J. Chem. Phys. **91**, 6533 (1989).
[3] J. M. Papanikolas, J. R. Gord, N. E. Levinger, D. Ray, V. Vorsa, and W. C. Lineberger, J. Phys. Chem. **95**, 8028 (1991).
[4] J. M. Papanikolas, V. Vorsa, M. E. Nadal, P. J. Campagnola, J. R. Gord, and W. C. Lineberger, J. Chem. Phys. **97**, 7002 (1992).
[5] J. M. Papanikolas, V. Vorsa, M. E. Nadal, P. J. Campagnola, H. K. Buchenau, and W. C. Lineberger, J. Chem. Phys. **99**, 8733 (1993).
[6] V. Vorsa, Ph.D. thesis, University of Colorado, Boulder, 1996.
[7] V. Vorsa, P. J. Campagnola, S. Nandi, M. Larsson, and W. C. Lineberger, J. Chem. Phys. **105**, 2298 (1996).
[8] V. Vorsa, S. Nandi, P. J. Campagnola, M. Larsson, and W. C. Lineberger, J. Chem. Phys. **106**, 1402 (1997).
[9] S. Nandi, A. Sanov, N. Delaney, J. Faeder, R. Parson, and W. C. Lineberger, J. Phys. Chem. A **102**, 8827 (1998).
[10] A. Sanov, S. Nandi, and W. C. Lineberger, J. Chem. Phys. **108**, 5155 (1998).
[11] A. Sanov, T. Sanford, S. Nandi, and W. C. Lineberger, J. Chem. Phys. **111**, 664 (1999).
[12] A. E. Johnson, N. E. Levinger, and P. F. Barbara, J. Phys. Chem. **96**, 7841 (1992).

[13] D. A. V. Kliner, J. C. Alfano, and P. F. Barbara, J. Chem. Phys. **98**, 5375 (1993).
[14] J. C. Alfano, Y. Kimura, P. K. Walhout, and P. F. Barbara, Chem. Phys. **175**, 147 (1993).
[15] I. Benjamin, P. F. Barbara, B. J. Gertner, and J. T. Hynes, J. Phys. Chem. **99**, 7557 (1995).
[16] P. K. Walhout, J. C. Alfano, K. A. M. Thakur, and P. F. Barbara, J. Phys. Chem. **99**, 7568 (1995).
[17] L. Perera and F. G. Amar, J. Chem. Phys. **90**, 7354 (1989).
[18] F. G. Amar and L. Perera, Z. Phys. D: At., Mol. Clusters **20**, 173 (1991).
[19] P. E. Maslen, J. M. Papanikolas, J. Faeder, R. Parson, and S. V. ONeil, J. Chem. Phys. **101**, 5731 (1994).
[20] J. M. Papanikolas, P. E. Maslen, and R. Parson, J. Chem. Phys. **102**, 2452 (1995).
[21] P. E. Maslen, J. Faeder, and R. Parson, Chem. Phys. Lett. **263**, 63 (1996).
[22] V. S. Batista and D. F. Coker, J. Chem. Phys. **106**, 7102 (1997).
[23] J. Faeder, N. Delaney, P. E. Maslen, and R. Parson, Chem. Phys. Lett. **270**, 196 (1997).
[24] N. Delaney, J. Faeder, P. E. Maslen, and R. Parson, J. Phys. Chem. A **101**, 8147 (1997).
[25] B. M. Ladanyi and R. Parson, J. Chem. Phys. **107**, 9326 (1997).
[26] J. Faeder and R. Parson, J. Chem. Phys. **108**, 3909 (1998).
[27] P. E. Maslen, J. Faeder, and R. Parson, Mol. Phys. **94**, 693 (1998).
[28] J. Faeder, N. Delaney, P. E. Maslen, and R. Parson, Chem. Phys. **239**, 525 (1998).
[29] C. J. Margulis and D. F. Coker, J. Chem. Phys. **110**, 5677 (1999).
[30] N. Delaney, J. Faeder, and R. Parson, J. Chem. Phys. **111**, 452 (1999).
[31] B. J. Greenblatt, M. T. Zanni, and D. M. Neumark, Science **276**, 1675 (1997).
[32] B. J. Greenblatt, M. T. Zanni, and D. M. Neumark, Faraday Discuss. **108**, 101 (1997).
[33] B. J. Greenblatt, M. T. Zanni, and D. M. Neumark, J. Chem. Phys. **111**, 10566 (1999).
[34] K. Asmis, T. Taylor, and D. M. Neumark, J. Chem. Phys. **109**, 4389 (1998).
[35] N. Delaney, J. Faeder, and R. Parson (private communication).
[36] W. C. Wiley and I. H. McLaren, Rev. Sci. Instrum. **26**, 1150 (1955).
[37] O. Cheshnovsky, S. H. Yang, C. L. Pettiette, M. J. Craycraft, and R. E. Smalley, Rev. Sci. Instrum. **58**, 2131 (1987).
[38] L.-S. Wang, H.-S. Cheng, and J. Fan, J. Chem. Phys. **102**, 9480 (1995).
[39] A. W. Castleman, Jr. and K. H. Bowen, Jr., J. Phys. Chem. **100**, 12911 (1996).
[40] M. T. Zanni, V. S. Batista, B. J. Greenblatt, W. H. Miller, and D. M. Neumark, J. Chem. Phys. **110**, 3748 (1999).
[41] Y. Zhao, C. C. Arnold, and D. M. Neumark, J. Chem. Soc., Faraday Trans. **89**, 1449 (1993).
[42] D. W. Arnold, S. E. Bradforth, E. H. Kim, and D. M. Neumark, J. Chem. Phys. **102**, 3510 (1995).
[43] D. W. Arnold, S. E. Bradforth, E. H. Kim, and D. M. Neumark, J. Chem. Phys. **102**, 3493 (1995).